WIDE-ANGLE ELECTRON DETECTOR

G. I. VOLKOV, K. I. GRINGAUZ, I. N. ZYDEL, L. P. SMIRNOVA and N. M. SHUTTE
Space Research Institute of U.S.S.R. Academy of Sciences, Moscow, U.S.S.R.
H. BARTHE, F. COTIN, J. L. MEDALE and H. RÈME
CESR, University of Toulouse, France

Abstract. The design, functioning, and main calibration, characteristics of a wide-angle detector, capable of recording electrons with energies $\geqslant 8$ keV and insensitive to u.v. solar radiation are described. A description of the sensor (electron trap) and its electronics in the analog (DEGAFOC) and counting (DEGAFOI) modes is given. Examples of telemetry recordings, illustrating the operation of the detector are included.

1. Introduction

The motion of artificially injected electrons along one of the Earth's magnetic field lines and mirrored from the conjugate point is influenced by plasma, by electron diffusion across the magnetic field, and by drift in the azimuthal direction, pitch angle diffusion, etc. When an electron beam moves along a field line it loses part of its energy and intensity as a result of scattering by neutral particles of the environment and by plasma inhomogeneities [1, 2].

During the preparation stage of the ARAKS experiment, we decided to develop a highly sensitive wide-angle detector, capable of recording weak electron fluxes, with energies exceeding approximately 10 keV, and insensitive to the solar u.v. background radiation at altitudes of 100–200 km in the atmosphere. The wide-angle detectors available at the time, e.g. charged particle traps [3] or solid state detectors [4], were inadequate since they were not sensitive enough, especially at energies less than 20 keV.

Thus, it was suggested that wide-angle traps should be developed making use of microchannel plates (MCP) covered by a protective metal film. It will be shown below that with the use of an MCP-cascade arrangement with a protective metal film on the input surface of the first plate, together with a proper selection of gain coefficients of the first and second plates, the device can be developed having parameters substantially differing from those described in [5, 6]. The detector is insensitive to solar electromagnetic radiation but sensitive to charged particles.

2. Sensor Description

2.1. Sensor design

The sensor is a wide-angle electron trap of the integral type with a system of axi-symmetrical flat electrodes (Figure 1). The aperture of the trap is covered by a grid (1) at the electrical potential of the body. The grid prevents ionospheric ions from entering the trap (2) and a special screen grid (3), separated from the trap's

Space Science Instrumentation **4** (1978) 189–199.

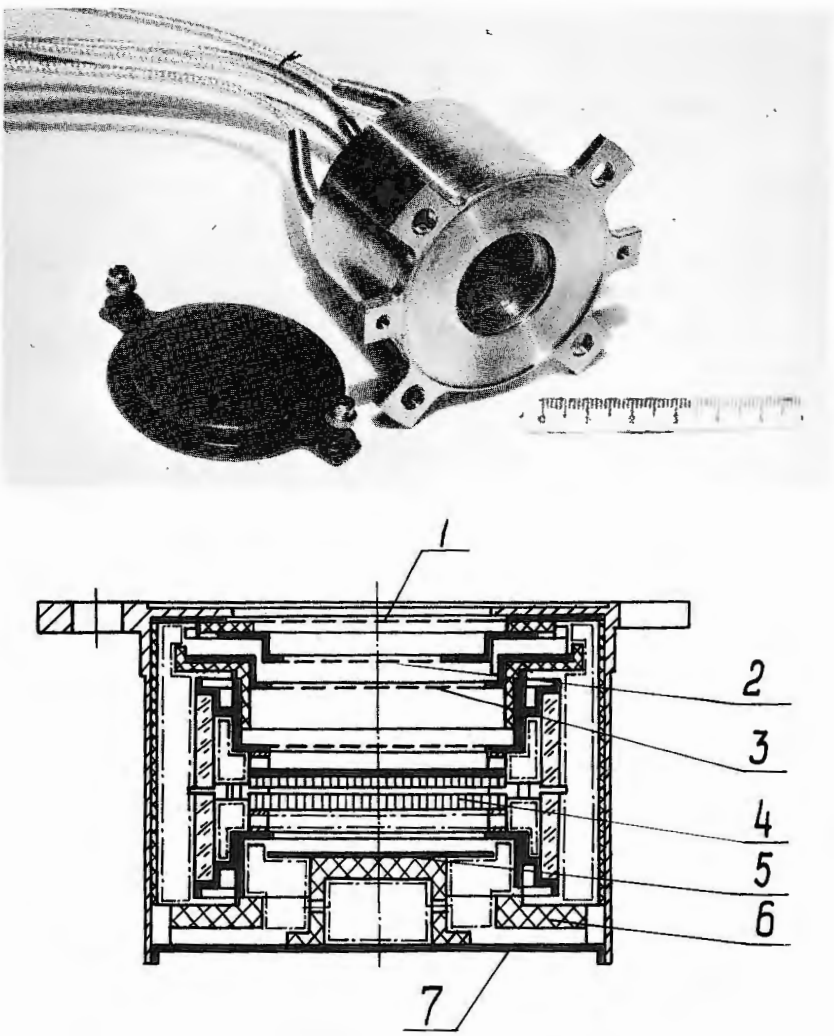

Fig. 1. Photograph and cross-sectional view of the wide-angle detector.

body by rings of fluoro plastic (6) is made of gold-plated tungsten with a total transmission coefficient of 75%. The MCP-multiplier (4) is mounted in the trap body in a special mandrel providing for fast evacuation of the area between the plates. A nickel plate collector (5) is located at the MCP-multiplier output. The trap body is welded from stainless steel. For installation of the trap on board the vehicle a mounting flange was provided. All terminals are brought out through the body front panel. We calculated that the trap evacuates to a level of 10^{-5} mmHg within 0.6 s. A programmer provides for switch-on of the onboard detector 130 s into the flight when the environmental pressure is considerably lower than the value of 10^{-5}.

2.2. MICROCHAN

A microchannel p
a large input surfa
surface can be co

The MCP is a s
into a honeycomb
coefficient of ~0.
an effective area
plates in series le
10^7. The recordin

Aluminum was
which allows a hig
a film thickness of
detector under irr
of the same inter
rate and the x-ax
are shown for thr
level of the elect

It is seen from F
u.v. radiation curv

Fig. 2. Dependence
with $P_{in} \approx 6 \times 10^6$ for

2.2. MICROCHANNEL PLATE MULTIPLIER

A microchannel plate (MCP) was chosen as the sensitive element because (i) it has a large input surface providing a high geometry factor for the trap, and (ii) the input surface can be covered with a protective aluminum film.

The MCP is a set of parallel channels with a diameter of about 20 μm combined into a honeycomb structure with a total number of channels of 10^6 and a filling coefficient of ~ 0.75 [8]. The plate thickness is 2 mm with a diameter of 28 mm and an effective area of ~ 4.5 cm^2. The gain factor of the plate is 10^3–10^4. Putting two plates in series leads to an increase in gain and provides an overall gain of about 10^7. The recording efficiency for electrons is between 10 and 20%.

Aluminum was used as a spraying material because of its relatively low density which allows a high transmittance for electrons with energies higher than 5 keV with a film thickness of about 3000 Å. Figure 2 shows the counting characteristics of the detector under irradiation by electrons (solid lines) and u.v. radiation at $\lambda \approx 1216$ Å of the same intensity $\sim (3\text{–}4) \times 10^6$ cm^{-2} s^{-1}. The y-axis represents the counting rate and the x-axis gives the values of the output plate supply voltage U_2. Curves are shown for three values of the first plate supply voltage, U_1. The discrimination level of the electronics corresponds to an output current of 8 μA.

It is seen from Figure 2 that the curves for electrons are shifted with respect to the u.v. radiation curves by 200–300 V. At the same voltage, the electron counting rate

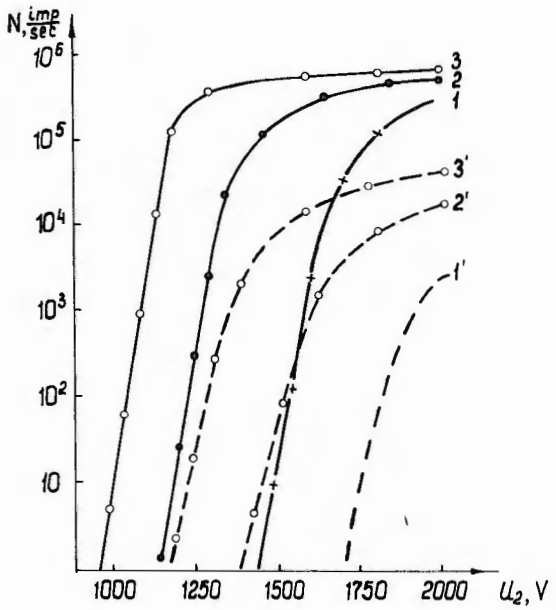

Fig. 2. Dependence of counting rate of the wide-angle detector on supply voltage of the output plate with $P_{in} \approx 6 \times 10^6$ for electrons (solid curves) and u.v. radiation (dashed curves) for $U_1 = \text{const.} = 1400$ V (1), 1600 V (2), 2000 V (3).

exceeds the u.v. counting rate by more than 5 orders of magnitude in the 'linear' part of the characteristics and by 1.5 orders in the deep saturation region.

This shift in counting characteristic of electrons and u.v. is associated with the difference in interaction of these radiations with the emitting surface of the microchannel walls, and, depending on chosen values of U_1 and U_2, can strongly influence the output parameters of the device [9].

Figure 3 shows the amplitude current pulse distribution at the collector versus MCP supply voltage when its input surface is irradiated by electrons (solid curves) and u.v. (dashed curves) of the same intensity. An increase in the plate supply voltage increases the multiplier electron current gain, with the amplitude distribution peak shifting towards the larger values and the signal dispersion diminishing to a value of 0.2–0.3. In the case of u.v., no amplitude distribution peak is observed. This feature is used for setting the discrimination threshold.

The protective film, together with the selection of the discrimination threshold and the detector plate voltage (for example, $U_1 \approx 1600$ V, $U_2 \approx 1250$ V) ensures that the

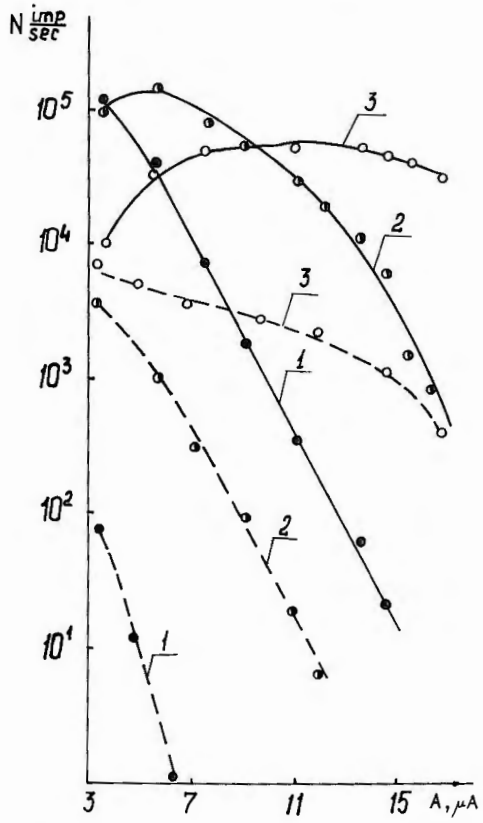

Fig. 3. Output current pulse distribution of the microchannel multiplier for radiation by electrons (solid curves) and u.v. (dashed curves) depending on supply voltage ($U_1 = 1400$ V), $U_2 = 1400$ V (1), 1600 V (2), 2000 V (3).

detector, in fact, does not record the solar electromagnetic radiation, but is rather sensitive to electrons.

2.3. Calibration characteristics

Figure 4 shows the counting rate (1) and the output current (2), as a function of the input electron flux P_{in} for two detectors operating in the pulse mode (DEGAFOI), and the current (DEGAFOC) mode, respectively.

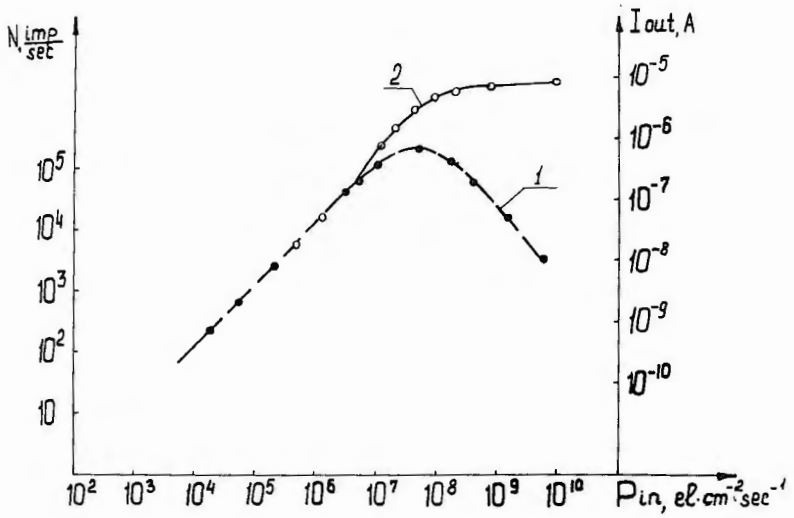

Fig. 4. Dependence of DEGAFOI counting rate (1) and DEGAFOC output current (2) on the input electron flux P_{in}.

The calibration characteristics were taken in a vacuum chamber with a pressure of 10^{-6} mmHg. A gun with a directly heated tungsten cathode was used as the electron source. A hydrogen gas-discharge lamp was used with a LiF window with a peak intensity of 2×10^{11} photons/s in the wavelength region around 1216 Å. The background level from u.v. radiation is less than 1–5 counts/s ($I \leqslant 10^{-11}$ A). In varying the input flux from 10^3 to 5×10^7 electron cm^{-2} s^{-1}, the counting rate and the detector output current changes from 10 to 2.5×10^5 count/s and from 10^{-11} to 3×10^{-6} A, respectively. Further increasing the input flux smoothly reduces the counting rate of the DEGAFOI detector, reaching 10^3 count/s with $P_{in} = 10^{10}$ electron cm^{-2} s^{-1}, and the detector output current approaches the saturation limit of the microchannel plate, (8×10^{-6} A).

The telemetry signal for the two detectors varies linearly: 5 V TM corresponds to a counting rate of 256 pulse/ms. The telemetry resolution allows signals of 0.02 V to be measured with sufficient accuracy, corresponding to a counting rate of 1 pulse/ms.

Figure 5 shows the angular response of the instrument. One must bear in mind that if the incident electron number flux is low, close to the sensitivity threshold of the device, then, in fact, the angular response is narrower than shown in Figure 5; (the registration of electrons ceases at rather small angles of particle incidence – for example, at a level of about 0.8).

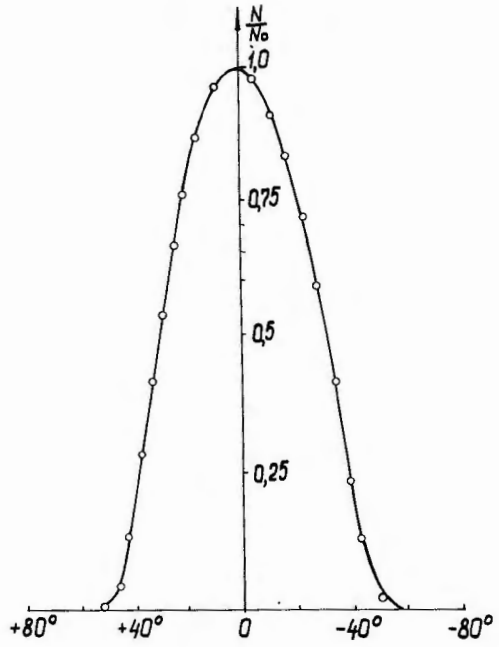

Fig. 5. Angular response of the wide-angle detector.

3. Electron Counting Circuitry

3.1. DEGAFOC ELECTRONICS

The analog electronics includes a high-voltage power supply with a resistance bridge to bias the detector, a current-to-frequency converter, counting and readout registers for the serial output of the information to the PCM telemetry encoder and voltage regulators for the batteries. Figure 6 gives the block diagram.

The high-voltage power supply consists of a d.c.–d.c. converter 28–3 000 V, 3 W. The high-voltage part was vacuum-potted in order to avoid internal breakdown during operation in a vacuum. The detector unit is biased through a chain of resistors each of which can take 2 000 V. The values of the bias voltages were adjusted to minimize the effects of ultraviolet radiation on the detector unit.

The current-to-frequency conversion: The detector signal current is converted into a pulse rate by a current-to-frequency converter similar to Shapiro's [12]. The usable range of the converted current is from 10^{-11} to 3×10^{-6} A. The transfer function of

the converter is given in Figure 7. The current-to-frequency converter consists of an integrating amplifier using low-loss capacitor C. The output voltage of the amplifier represents the time integral of the input current. When this voltage is equal to the reference voltage $V_{ref\,1}$ of Comparator 1, the latter is triggered. This releases a monostable which provides a blocking pulse of constant amplitude and duration to

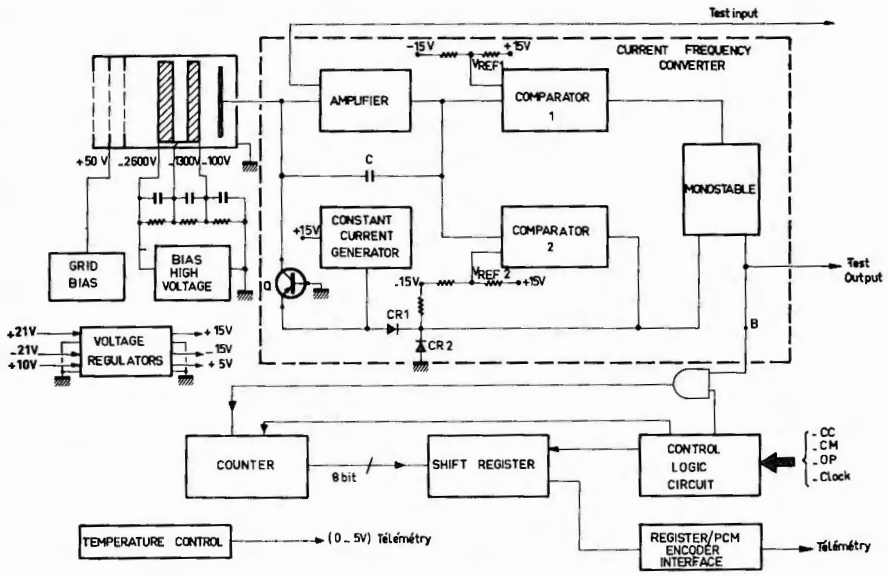

Fig. 6. Block diagram of DEGAFOC detector electronics.

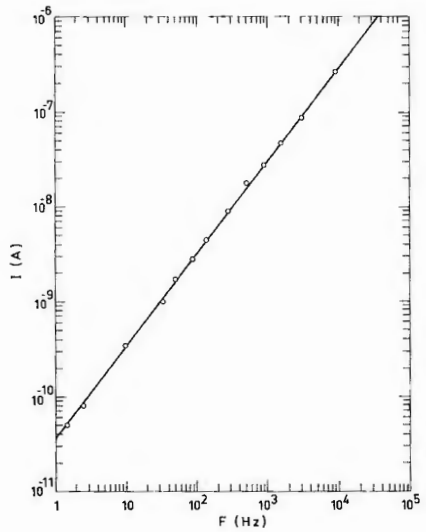

Fig. 7. The transfer function of analog-to-frequency converter of the DEGAFOC detector.

diodes CR_1 and CR_2. Transistor Q then applies the constant current to the amplifier input. Thus, a fixed charge is delivered to capacitor C. The output voltage of the amplifier is reduced, resetting Comparator 1 to zero, and the integration cycle can begin again. If the current of the detector unit exceeds 3 μA, Comparator 2 sends an overload pulse, reducing the output voltage of the amplifier. Thus, the converter can never remain saturated.

Output logic (Figure 8): The pulses from the current-to-frequency converter are taken from point B in Figure 6 and counted directly in an 8-bit counting register ($IC_1 + IC_2$). Signals supplied by the PCM telemetry encoder permit the synchronous operation of all experiments. The time diagram in Fig. 3 of [10] gives the timing of these signals. Every millisecond, the count rate is blocked for 2 μs in order to allow the transfer of information contained in counters IC_1 and IC_2 to the readout registers IC_3 and IC_4. The blocking and transfer signals are generated by a coincidence between the word synchro and short cycle signals. The blocking is performed by gate P_1. After information transfer, the monostable IC_3 resets the IC_1 and IC_2 counters to zero. The coincidence of signals OP_1 and Clock permit the information contained in the IC_3 and IC_4 registers to be read out serially to the telemetry.

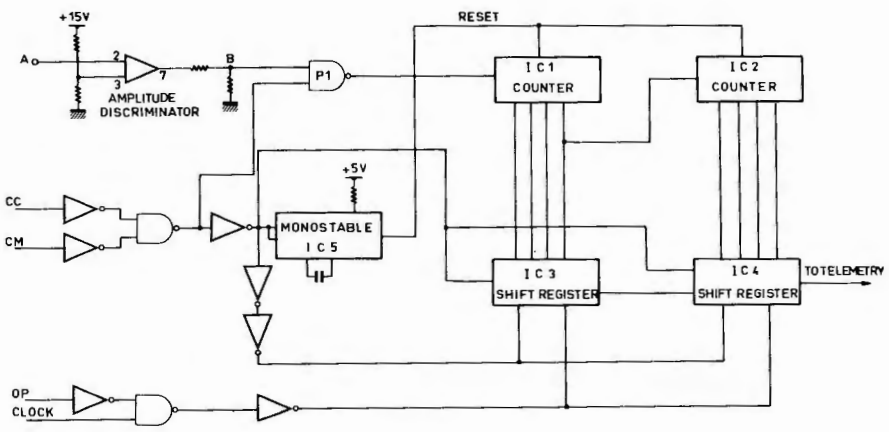

Fig. 8. Output logic of DEGAFOC and DEGAFOI detectors.

3.2. DEFAGOI ELECTRONICS

This detector consists of a detector unit identical to that of the DEGAFOC, but with different electronics. It is used to analyze low electron fluxes in a wide solid angle. The block diagram is given in Figure 9. The electronics includes a high-voltage power supply with its resistor bridge for biasing the detection block, an amplifier and an amplitude discriminator, count and readout registers for transmitting information to the PCM telemetry, and voltage regulators.

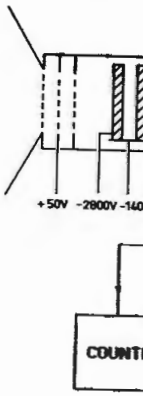

Fig. 9. Blo

The high-voltage p
only the bridge resisto
adjusted to minimize
Pulses from the dete
Lampton and Primbsc
integrated circuit cons
these is used as a ch
charge-to-voltage con
establishes the decay
amplifier is a variable-
fixed gain of −20. By
-10^{14} V/C.

Output logic: the pu
which shapes the pulse
follows is identical to t

Two instruments DEG
provided reliable recor
of 10^5–10^{10} electron cm
Figure 10 gives an e
injection of 140° relat
electron fluxes and follo
we see that the recorde

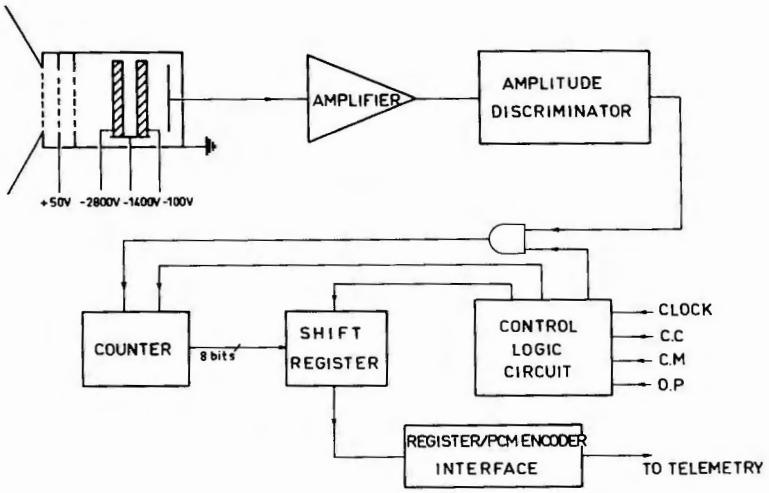

Fig. 9. Block diagram of the wide-angle pulse detector unit, DEGAFOI.

The high-voltage power supply is identical to that of the DEGAFOC detector; only the bridge resistor values are different. The voltages on the detector have been adjusted to minimize the effects of ultraviolet radiation on the detector count rate.

Pulses from the detector are amplified by means of an amplifier similar to that of Lampton and Primbsch [11], the operation of which is based on the principle of an integrated circuit consisting of three inverting amplifiers (Figure 2 of [10]). One of these is used as a charge amplifier; its feed-back capacitor C_3 determines the charge-to-voltage conversion again from this stage, and the feedback resistor R_4 establishes the decay time constant R_4C_3 of the amplified pulses. The second amplifier is a variable-gain stage controlled by resistor R_5. The third stage has a fixed gain of -20. By varying R_5, the amplifier gain can be adjusted from -10^{11} to -10^{14} V/C.

Output logic: the pulses from the amplifier enter the amplitude discriminator which shapes the pulses and separates them from the background. The logic which follows is identical to that of the DEGAFOC detector (Figure 8).

4. Conclusion

Two instruments DEGAFOC and DEGAFOI installed on board the Eridan rocket provided reliable recordings of electrons with energies above 8–9 keV and for fluxes of 10^5–10^{10} electron cm^{-2} s^{-1}. The acceptance angle is ±40°.

Figure 10 gives an example of the DEGAFOC signals recorded during beam injection of 140° relative to the rocket axis. The signals are given in terms of electron fluxes and follow exactly the periodicity of the gun pulses. From Figure 10, we see that the recorded electron flux varies by more than an order of magnitude

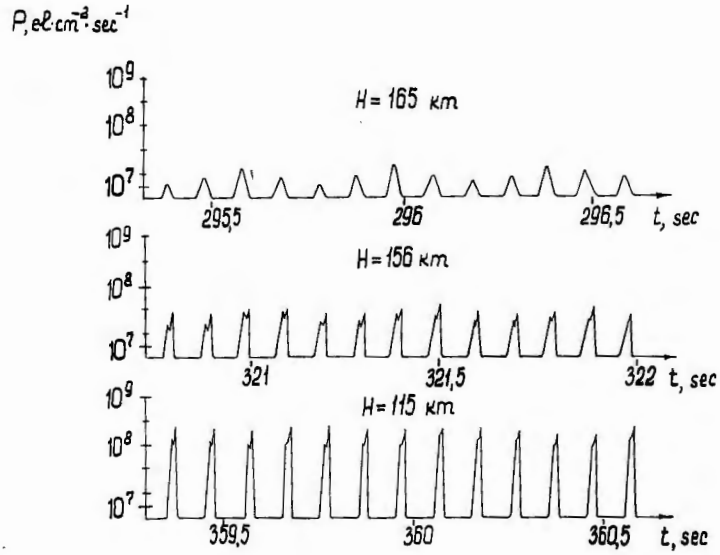

Fig. 10. DEGAFOC detector signals at the moment of beam injection under an angle of 140° with respect to the rocket axis for three rocket altitudes. The launch was directed towards the North.

between 165 and 115 km altitude. These signals are presumably caused by electrons entering the trap as a result of scattering by ambient neutral molecules. This data is in good agreement with the altitude dependence of the neutral component density [13]. Figure 11 represents DEGAFOI data of the flux of electrons naturally precipitating along magnetic field lines during pauses between pulses. This flux intensity changes depending on the detector pitch-angle which varies between 24°

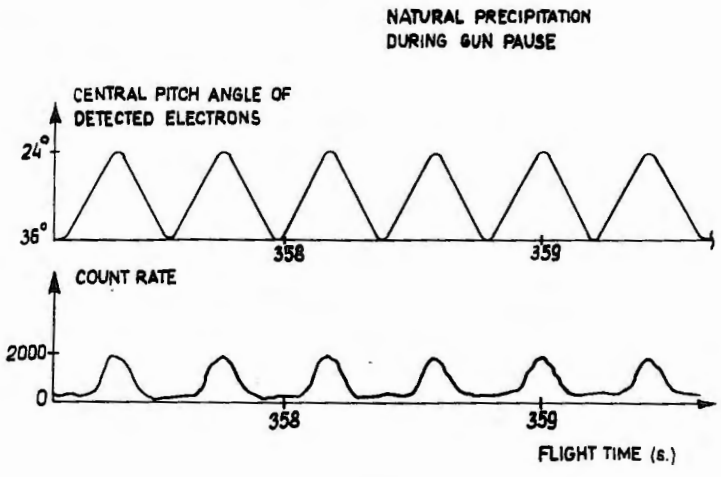

Fig. 11. Natural precipitation of radiation belt electrons recorded in pauses between pulses.

and 37° during the rocket spin period. At the maximum pitch-angle the precipitated electron flux is equal to 10^7 electron $cm^{-2}\,s^{-1}$.

The data obtained indicate the satisfactory operation of the detectors under actual experimental conditions.

References

1. Hendrickson, R. A., McEntire, R. W., and Winckler, J. R.: *Nature* **230**, 564 (1971).
2. Gendrin, R.: *Space Sci. Rev.* **15**, 6 (1974).
3. Gringauz, K. I.: *Space Res.* **2**, 539 (1961).
4. Applied spectrometry with semiconductor detectors, Moscow, Nuclear publication (1974).
5. Parkes, W., and Gott, R.: *Nucl. Instr. and Methods* **95**, 487 (1971).
6. Ruggieri, D. Y.: *IEEE Trans. Nucl. Sci.* **NS-19(3)**, 74 (1972).
7. McEntire, R. W., Hendrickson, R. A. and Winckler, J. R.: *J. Geophys. Res.* **79**, 16, 2343 (1974).
8. Volkov, G. I., Gringauz, K. I., et al., *Radiotecn. and Electr. (USSR)*, **xxi**, 8, 1715 (1976).
9. Smirnova, L. P. and Shutte, N. M.: DAN USSR, ser. Phys. **214**, 549 (1974).
10. Barthe, H., Cotin, F. and Reme, H.: *Space Sci. Instrum.*, this issue.
11. Lampton, M. and Primbsch, J. H.: *Rev. Sci. Instrum.* **42**, 5, 731 (1971).
12. Shapiro, E. G.: *IEEE Trans. Nucl. Sci.* **NS–17(1)**, 335 (1970).
13. Martini, L. and Shutte, H.: Cosmic Res. **1**, 719 (1973).